Microphase Separation in Poly(oxyethylene)−Poly(oxybutylene) Diblock Copolymers

Shao-Min Mai,*,† J. Patrick A. Fairclough,‡ Nicholas J. Terrill,‡,§ Simon C. Turner,‡ Ian W. Hamley,‖ Mark W. Matsen,⊥ Anthony J. Ryan,‡,§ and Colin Booth†

Manchester Polymer Centre and Department of Chemistry, University of Manchester, Manchester M13 9PL, U.K., Department of Chemistry, University of Sheffield, Sheffield S3 7HF, U.K., School of Chemistry, University of Leeds, Leeds LS2 9TJ, U.K., CCLRC Daresbury Laboratory, Warrington WA4 4AD, U.K., and Polymer Science Centre, University of Reading, Whiteknights, Reading RG6 6AF, U.K.

Received July 13, 1998; Revised Manuscript Received September 15, 1998

ABSTRACT: Twenty-six poly(oxyethylene)-poly(oxybutylene) diblock copolymers were prepared by anionic polymerization. The phase behavior of these copolymers was studied near the order−disorder transition over the composition range from 0.21 to 0.84 poly(oxyethylene) volume fraction. Small-angle X-ray scattering was used to characterize phase transition temperatures and ordered state symmetries. Four distinct microstructures were observed: body-centered cubic, hexagonally packed cylinders (hex), lamellae (lam), and a bicontinuous cubic phase with $Ia\bar{3}d$ symmetry, together with a less well-defined region of the phase diagram comprising either hexagonally perforated layers or biphasic hex and lam. The Flory−Huggins parameter as a function of temperature was estimated using both the mean-field approximation and a fluctuation correction to the mean-field theory. The experimental microphase behavior is compared with the exact mean-field phase diagram calculated using self-consistent-field theory.

1. Introduction

Diblock copolymers with narrow block length distributions may be readily prepared by sequential anionic polymerization of ethylene oxide followed by 1,2-butylene oxide. We denote these copolymers E_mB_n, where E represents an oxyethylene unit [OCH_2CH_2] and B an oxybutylene unit [$OCH_2CH(CH_2CH_3)$]. Since an E block is hydrophilic and a B block is hydrophobic, there has been recent interest in the self-association properties of copolymers of this type when dissolved in water.[1] Their bulk properties are of equal interest, since microphase-separated structures may form from the disordered melt when the temperature is lowered, either by crystallization of the E blocks[2−4] or by microphase separation in the melt state.[5] The latter occurs when the enthalpic cost of the unfavorable segment−segment interactions is sufficient to overcome the entropy loss of demixing the blocks to form an ordered structure.[6] The purpose of this paper is to report new results for the microphase separation of E_mB_n copolymers in the liquid state.

In our recent paper,[5] we reported the synthesis and phase behavior of 13 E_mB_n copolymers, which enabled definition of the order−disorder transition (ODT) boundary for the symmetrical case (volume fraction 0.5) and, using the mean-field approximation, determination of the temperature coefficient of the Flory−Huggins parameter χ. To fill out the phase diagram, we have synthesized 13 more diblock copolymers. Added to those with lamellar and hexagonal microphase-separated melts, described previously,[5] we now report copolymers with cubic-structured melts. Consequently, we are now able to describe the phase diagram for the E_mB_n system in more detail, and this enables closer comparison of the experiment with the state-of-the-art phase diagram calculated using self-consistent mean-field theory.[7,8]

* To whom correspondence should be addressed.
† University of Manchester.
‡ University of Sheffield.
§ CCLRC Daresburg Laboratory.
‖ University of Leeds.
⊥ University of Reading.

2. Experimental Section

2.1. Synthesis and Characterization. Diblock copolymers were prepared by sequential anionic polymerization of ethylene oxide (EO) followed by 1,2-butylene oxide (BO). Details of the methods have been published.[5] The monofunctional initiator was 2-(2-methoxyethoxy)ethanol activated by reaction with potassium metal, with the ratio [OH]/[OK] being adjusted to ensure a controlled rate of polymerization in the temperature range 45−65 °C. Vacuum-line and ampule techniques were used throughout. Characterization of the intermediate poly(oxyethylene) and the final copolymer was by gel permeation chromatography (GPC) and ^{13}C NMR spectroscopy: GPC (calibrated by poly(oxyethylene) standards) for distribution width; NMR for number-average molar mass, composition, and block structure. A summary of the molecular characteristics of the copolymers is given in Table 1: i.e., the formula in E_mB_n notation, the number-average molar mass (M_n), and the mole and weight fractions of oxyethylene units (x_E and w_E, respectively). All of the copolymers had narrow molar mass distributions: $M_w/M_n \leq 1.05$. The listing is in ascending order of x_E. All of the copolymers are included, with those previously described in ref 5 being indicated.

2.2. Time-Resolved Small-Angle X-ray Scattering (SAXS). SAXS measurements were made on a beamline 8.2 of the SRS at the CCLRC Daresbury Laboratory, Warrington, U.K.[9] The camera was equipped with a multiwire quadrant detector located 3.5 m from the sample position. Samples were placed in a TA Instruments differential scanning calorimetry (DSC) pan containing a 0.75-mm brass spacer ring and fitted with windows made from 25-μm-thick mica. The loaded pans were placed in the cell of a Linkam DSC of single-pan design. A complete description of the DSC and the sample pans, including calibration of the temperature scale, can be found elsewhere.[10,11] The temperature program was as follows: heat from room temperature to T_{ODT} + 30 °C at 10 °C min^{-1}, hold at the maximum temperature for 1 min, and cool at 10 °C min^{-1} to 10 °C. In some cases temperature ramps of 1 and 20

10.1021/ma981089k CCC: $15.00 © 1998 American Chemical Society
Published on Web 10/29/1998

Table 1. Molecular Characteristics of E_mB_n Block Copolymers[a]

copolymer	M_n/(g mol^{-1})	x_E	w_E
$E_{40}B_{79}$	7400	0.34	0.24
$E_{16}B_{22}$[b]	2300	0.42	0.31
$E_{50}B_{70}$	7200	0.42	0.30
$E_{47}B_{62}$	6500	0.43	0.32
$E_{68}B_{65}$	7700	0.51	0.39
$E_{64}B_{60}$	7100	0.52	0.40
$E_{115}B_{103}$[b]	12500	0.53	0.41
$E_{75}B_{54}$	7200	0.58	0.46
$E_{43}B_{23}$[b]	3400	0.65	0.53
$E_{85}B_{45}$	7000	0.65	0.54
$E_{100}B_{51}$	8100	0.66	0.55
$E_{36}B_{18}$[b]	2900	0.67	0.55
$E_{56}B_{27}$[b]	4400	0.67	0.56
$E_{60}B_{29}$[b]	4700	0.67	0.56
$E_{76}B_{38}$[b]	6100	0.67	0.55
$E_{96}B_{47}$[b]	7600	0.67	0.56
$E_{114}B_{56}$[b]	9000	0.67	0.55
$E_{155}B_{76}$[b]	12300	0.67	0.55
$E_{35}B_{12}$[b]	2400	0.74	0.64
$E_{110}B_{30}$	7000	0.79	0.69
$E_{131}B_{35}$	8300	0.79	0.70
$E_{209}B_{45}$[b]	12400	0.82	0.74
$E_{49}B_9$[b]	2800	0.84	0.77
$E_{134}B_{19}$	7300	0.88	0.81
$E_{290}B_{33}$	15100	0.90	0.84
$E_{290}B_{30}$	14900	0.91	0.86

[a] $x_E = m/[m + n]$ and $w_E = m/[m + n(72/44)]$. [b] Previously described in ref 5.

°C min^{-1} were also applied to check for heating rate effects. The data acquisition system[11] had a time-frame generator which collected the data in 6-s frames separated by a wait time of 10 μs. The scattering pattern from an oriented specimen of wet collagen (rat-tail tendon) was used for calibration. The experimental data were corrected for background scattering (subtraction of the scattering from the camera, hot stage, and an empty cell), sample thickness and transmission, and any departure from the positional linearity of the detector.[12] Results are presented in terms of the wave vector $q = (4\pi/\lambda)\sin(\theta/2)$, where the wavelength $\lambda = 1.54$ Å and θ is the scattering angle.

3. Results and Discussion

The copolymers marked in Table 1 were investigated previously.[5] Some minor changes in the formulas arise from their recharacterization by ^{13}C NMR, but all of the changes are within ±1 B unit and ±2 E units, i.e., within experimental error. In this section attention is concentrated on the properties of the newly synthesized copolymers.

3.1. Microphase Structures and Order−Disorder Transition Temperatures. Figures 1 and 2 show SAXS patterns from copolymer melts which illustrate the cubic phase with $Im\bar{3}m$ symmetry (body-centered cubic, bcc) of copolymer $E_{40}B_{79}$ at 35 °C and the bicontinuous cubic phase with $Ia\bar{3}d$ symmetry (gyroid, gyr) of copolymer $E_{75}B_{54}$ at 70 °C. The data are presented as log(intensity) versus normalized wave vector, q/q^*, where q^* is the value of q at the peak of the first-order reflection, and the characteristic spacings of the bcc and gyr structures are marked.

The phase behavior of copolymer $E_{75}B_{54}$ is illustrated in more detail in Figure 3, which shows a three-dimensional relief diagram of time-resolved SAXS data obtained during heating and cooling of the copolymer. The heating and cooling cycle was 10 °C → 150 °C → 10 °C at a ramp rate of 10 °C min^{-1}. The plot shows log(intensity) versus scattering vector, q, versus temperature, T. The SAXS pattern at low temperature (four equally spaced reflections) is consistent with a lamellar (lam) semicrystalline phase that, at intermediate temperature ($63 \le T \le 126$ °C), confirms the gyroid phase (see Figure 2), while the broad scattering peak at high temperatures ($T > 126$ °C) indicates a disordered melt with composition fluctuations. The phase sequence is reversed on cooling.

Heating and cooling experiments, such as those that are illustrated in Figure 3, were used to locate the

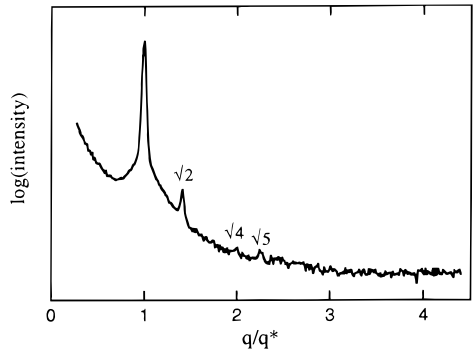

Figure 1. SAXS patterns for molten copolymer $E_{40}B_{79}$ at 35 °C. q^* is the value of q at the peak of the first-order reflection. The logarithmic intensity scale is arbitrary. Reflections at $q/q^* = 1, \sqrt{2}, \sqrt{4}$, and $\sqrt{5}$ indicate a body-centered cubic phase.

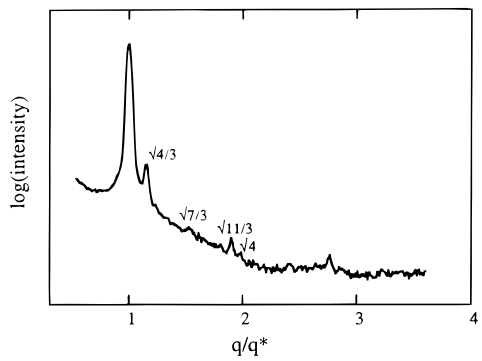

Figure 2. SAXS patterns for molten copolymer $E_{75}B_{54}$ at 70 °C. q^* is the value of q at the peak of the first-order reflection. The logarithmic intensity scale is arbitrary. Reflections at $q/q^* = 1, \sqrt{4/3}, \sqrt{7/3}, \sqrt{8/3}, \sqrt{10/3}, \sqrt{11/3}$, and $\sqrt{12/3}$ indicate a gyroid phase.

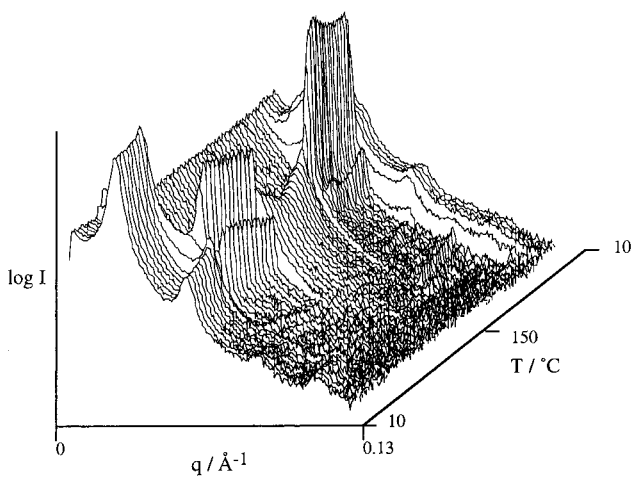

Figure 3. Three-dimensional relief diagram of time-resolved SAXS data obtained with a time resolution of 6 s while heating and cooling copolymer $E_{75}B_{54}$. The plot shows log(intensity) versus scattering vector, q, versus temperature, T. The thermal cycle was 10 °C → 150 °C → 10 °C at a ramp rate of 10 °C min^{-1}.

Table 2. Liquid-State Properties of E_mB_n Copolymers: $T \geq 50$ °C

copolymer	r_v[a]	ϕ_E[b]	structure[c] (70 °C)	d/Å[d] (70 °C)	ODT/°C[e]
$E_{40}B_{79}$	189	0.210	bcc (50 °C)	104 (50 °C)	60
$E_{50}B_{70}$	182	0.270	hex	114	112
$E_{16}B_{22}$	58	0.280	dis		
$E_{47}B_{62}$	164	0.286	hex	104	93
$E_{68}B_{65}$	191	0.356	hex	126	140
$E_{64}B_{60}$	177	0.361	hex	119	126
$E_{115}B_{103}$	310	0.371	hex	177	225
$E_{75}B_{54}$	177	0.424	gyr	123	126
$E_{43}B_{23}$	86	0.497	lam	*f*	43[f]
$E_{85}B_{45}$	170	0.500	lam	119	140
$E_{100}B_{51}$	196	0.509	lam	131	165
$E_{36}B_{18}$	70	0.514	dis		
$E_{76}B_{38}$	148	0.514	lam	109	114
$E_{96}B_{47}$	185	0.519	lam	127	163
$E_{114}B_{56}$	220	0.519	lam	146	210
$E_{155}B_{76}$	299	0.519	lam	174	270
$E_{56}B_{27}$	107	0.523	lam (50 °C)	89 (50 °C)	53[f]
$E_{60}B_{29}$	115	0.523	lam (50 °C)	93 (50 °C)	60
$E_{35}B_{12}$	58	0.607	dis		
$E_{110}B_{30}$	167	0.660	lam	115	85
$E_{131}B_{35}$	197	0.664	lam	138	133
$E_{209}B_{45}$	294	0.711	lam	180	190[g]
$E_{49}B_9$	66	0.742	dis		
$E_{134}B_{19}$	170	0.789	dis		
$E_{290}B_{33}$	352	0.820	hex	175	160
$E_{290}B_{30}$	347	0.840	hex	163	152

[a] $r_v = m + (72/44)(1.067/0.923)n = m + 1.89n$, with 0.923 and 1.067 g cm^{-3} being the limiting specific volumes of liquid poly(oxyethylene) and poly(oxybutylene) at 70 °C: see ref 13. [b] $\phi_E = m/[m + 1.89n]$ where 1.89 is the ratio of limiting specific volumes: see footnote *a*. [c] lam = lamellar; hex = hexagonal (cylinders); bcc = body-centered cubic (spheres, $Q_{Im\bar{3}m}$); gyr = gyroid (bicontinuous cubic phase, $Q_{Ia\bar{3}d}$); dis = disordered. [d] d = periodicity from SAXS when the sample is heated. [e] ODT = order–disorder transition temperature from SAXS. [f] Data for supercooled melt. *d*-spacing not measured for copolymer $E_{43}B_{23}$. Temperatures are for the disorder–order transition (DOT) from SAXS during cooling. [g] $E_{209}B_{45}$ has an order–order transition, lam → gyr, at 150 °C (see text for details). The ODT listed is for gyr → dis.

temperature of the ODT. In fact, as described previously,[5] the ODT was defined not only from the step change in the peak-maximum intensity (see Figure 3) but also from discontinuous changes in peak width and peak shape.

The structure observed by SAXS, the periodicity ($d = 2\pi/q^*$) of the phase at 70 °C (unless noted otherwise), and the temperature at which the melt disordered (ODT) are listed for each copolymer (where applicable) in Table 2. Included in Table 2 are the volume fraction of the oxyethylene block in the liquid state at 70 °C (ϕ_E) and the overall length of the copolymer molecule in segments (r_v), taking the segment volume to be that of an E unit. The listing is in ascending order of ϕ_E. Given the reported temperature dependences of specific volume (v_{sp}),[13] the ratio $v_{B,sp}/v_{E,sp}$, which is used in calculating r_v and ϕ_E (see Table 2), is predicted to vary only slightly within the temperature range of the ODTs, i.e., from 1.156 at 60 °C to 1.151 at 270 °C. This small variation had an insignificant effect on the phase diagrams discussed in section 4 and was ignored, with the equations used to calculate r_v and ϕ_E from the formulas of the copolymers being

$$r_v = m + 1.89n \tag{1}$$

and

$$\phi_E = m/[m + 1.89n] \tag{2}$$

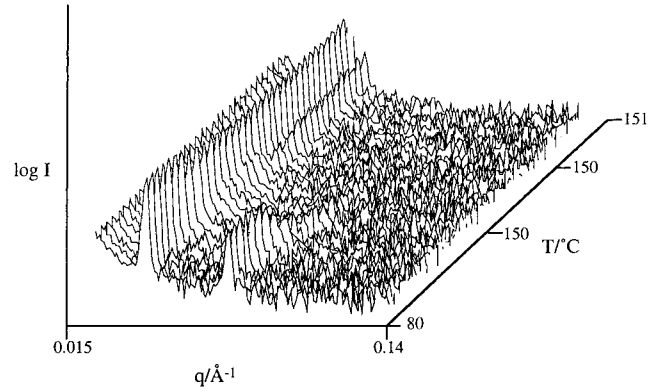

Figure 4. Three-dimensional relief diagram of time-resolved SAXS data obtained with a time resolution of 6 s while heating copolymer $E_{209}B_{45}$. The plot shows log(intensity) versus scattering vector, *q*, versus temperature, *T*. The program was heated from 80 to 150 °C at 50 °C min^{-1}, held for 1 min, and heated to 151 °C at 1 °C min^{-1}.

Details can be found in Table 2.

The E_mB_n system has a crystal–melt boundary at low temperature. Because of this, the lower limit for investigation of the melt state was T = 40–65 °C depending on chain length and composition, as described in detail elsewhere.[3,4] In fact, the structures determined at 50 °C for three of the copolymers ($E_{40}B_{79}$, $E_{56}B_{27}$, and $E_{60}B_{29}$) were for supercooled melts.

3.2. Order–Order Transition (OOT) of $E_{209}B_{45}$. A three-dimensional relief diagram of time-resolved SAXS data obtained while heating copolymer $E_{209}B_{45}$ is shown in Figure 4. The heating program in this experiment was 80–150 °C at 50 °C min^{-1}, hold at 150 °C for 1 min, and then heat at 1 °C min^{-1}. A liquid-state order–order transition from lamella to gyroid at ca. 150 °C is apparent. The ODT (gyroid to disorder, not shown in the figure) was 190 °C

3.3. Order–Order and Order–Disorder Transitions of Blends. To investigate the transition region between the lamellar and hexagonal structures at low ϕ_E, eight blends of copolymers $E_{155}B_{76}$ (ϕ_E = 0.519) and $E_{115}B_{103}$ (ϕ_E = 0.371) were made, as shown in Table 3 where the nomenclature (blend 40, etc.) indicates the volume percent of E in the blend. This blending technique has been successfully used by others to map in detail the ODT and OOT lines[14,15] and is supported theoretically.[16] Investigation by SAXS showed that some of the blends exhibited order–order transitions in the melt. Examples of scattering patterns above and below the OOT are shown in Figures 5 (blend 42) and 6 (blend 46). Blend 42 melted to give a hexagonal phase which transformed on heating to a gyroid phase. The interpretation of the scattering pattern from blend 46 at a temperature (100 °C) below the OOT (see Figure 6) is less certain, possibly from a hexagonally perforated lamellar (hpl) phase[17–19] or possibly from coexisting hexagonal and lamellar phases. We note that stable coexistence regions are possible in blends, although they are not permitted in neat diblock copolymer systems. With regard to this point, we have evidence from simultaneous rheology/SAXS that copolymer $E_{209}B_{45}$ on heating under shear does form an hpl phase between its lam and gyr phases, although there is no evidence that the phase is stable.[20]

The OOT and ODT temperatures for all of the blends, shown in Table 3, were used to construct the phase diagrams discussed in section 4.

Table 3. Transition Temperatures of Blends of Copolymers $E_{155}B_{76}$ and $E_{115}B_{103}$[a]

sample	wt % $E_{115}B_{103}$	ϕ_E	r_v	T_{OOT}/°C	T_{ODT}/°C
blend 40	83	0.40	308	172 (hex → gyr)	237 (gyr → dis)
blend 42	69	0.42	306	142 (hex → gyr)	240 (gyr → dis)
blend 43	63	0.43	306	142 (hex → gyr)	238 (gyr → dis)
blend 44	56	0.44	305	139 (hpl or biphasic → gyr)	240 (gyr → dis)
blend 45	49	0.45	304	132 (hpl or biphasic → gyr)	242 (gyr → dis)
blend 46	43	0.46	303	151 (hpl or biphasic → gyr)	246 (gyr → dis)
blend 48	29	0.48	302		255 (lam → dis)
blend 50	17	0.50	300		258 (lam → dis)

[a] See footnotes to Table 2 for definition of quantities and structures. See text for discussion of the uncertain morphology (hpl or biphasic).

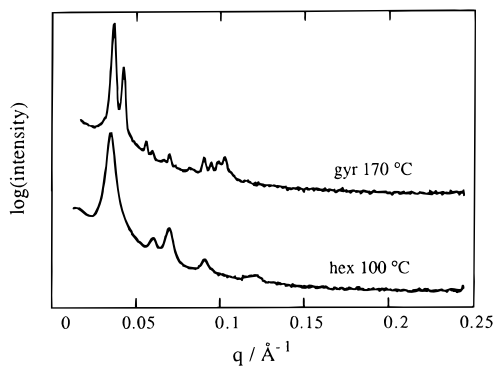

Figure 5. SAXS patterns for a blend ($\phi_E = 0.42$) of copolymers $E_{155}B_{76}$ and $E_{115}B_{103}$ at 100 and 170 °C. The logarithmic intensity scale is arbitrary.

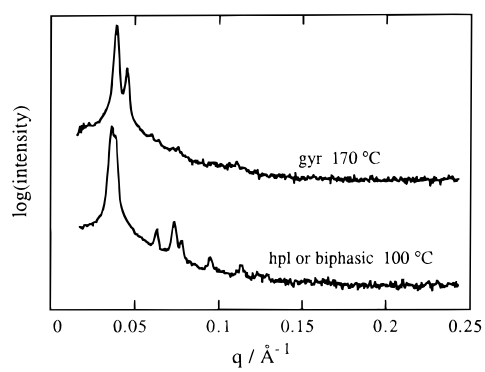

Figure 6. SAXS patterns for a blend ($\phi_E = 0.46$) of copolymers $E_{155}B_{76}$ and $E_{115}B_{103}$ at 100 and 170 °C. The logarithmic intensity scale is arbitrary. The assignment of the lower scattering curve is uncertain, since either an hpl phase or mixed hex and lam phases (biphasic) would fit the pattern: see text for discussion.

3.4. Temperature Dependence of χ. To locate the copolymers on the conventional phase diagram (χr_v versus ϕ_E), the value of χ is required as a function of temperature, i.e., the coefficients in equation $\chi = \alpha + \beta/T$. The accumulated data for symmetrical copolymers ($\phi_E \approx 0.5$) were used to calculate χ using the mean-field approximation for its critical value for microphase separation,[21]

$$(\chi r_v)_c = 10.5 \qquad (3)$$

These values are plotted against the reciprocal of the transition temperature in Figure 7. The least-squares fit to the data gives

$$\chi = 48.0/T - 0.0535 \qquad (4)$$

which is very similar to the relationship reported previously.[5] The segment volume v_E is 42 cm^3 mol^{-1} at 100 °C.

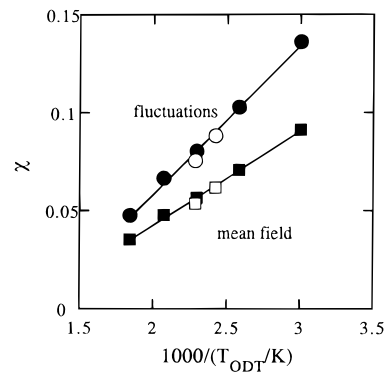

Figure 7. Values of the Flory−Huggins interaction parameter at the ODT calculated either from eq 3 (mean field) or from eq 5 (fluctuations) versus reciprocal transition temperature for symmetrical copolymers. The solid lines are least-squares fits to the data points.

The nature of the SAXS patterns observed for the disordered phase (see refs 3 and 5 for examples) confirms that the ODT is a transition from an ordered melt to a fluctuating melt; hence, using mean-field theory will lead to an underestimate of the value of χ. Repeating the exercise for the $\phi_E \approx 0.5$ copolymers but using Fredrickson and Helfand's expression for a fluctuating melt[22]

$$(\chi r_v)_c = 10.5 + 41\bar{N}^{-1/3} \qquad \bar{N} = r_v b^6 \rho^2 \qquad (5)$$

with approximate values for the segment statistical length ($b \approx 5.3 \times 10^{-10}$ m) and number density ($\rho \approx 1.4 \times 10^{28}$ m^{-3}) gives (see Figure 7)

$$\chi = 75.6/T - 0.0929 \qquad (6)$$

The value of $b = 5.3 \times 10^{-10}$ m used in the calculation is an appropriately weighted average of values reported previously for poly(oxyethylene) and poly(oxybutylene) segments.[23,24] Conflicting values have been reported for poly(oxyethylene):[25] the value used is supported by rotational-isomeric state calculations.[26] In a future paper we will report an investigation of fluctuation effects, using a combination of X-ray and neutron scattering and rheology, and thereby obtain a more certain determination of χ.

4. Phase Diagrams

4.1. Phase Boundaries. The results listed in Tables 2 and 3 were used to define the phase boundaries shown in Figure 8, i.e., on a plot of χr_v against ϕ_E, with the necessary quantities calculated using equations 1, 2, and 6 (i.e., χ calculated for the fluctuating melt). The filled circles denote ODTs while the open circles signify OOTs. With an increase in χr_v (i.e., on cooling) and with the exception of the gyroid phase, all structured phases

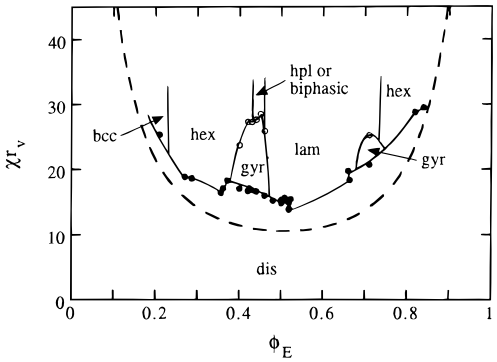

Figure 8. Phase diagram (χr_v versus ϕ_E) constructed using χ given by eq 6. The filled circles denote order−disorder transitions (ODT) and the open circles order−order transitions (OOT). The solid curves have been drawn to indicate the different phases observed but do not correspond to precise phase boundaries. Regarding the hpl/biphasic region, if hpl, it presumably represents a metastable state, while if biphasic, it presumably results from using blends to map out the complex phase region. The dashed curve is the boundary predicted by self-consistent mean-field theory. See text for a detailed discussion.

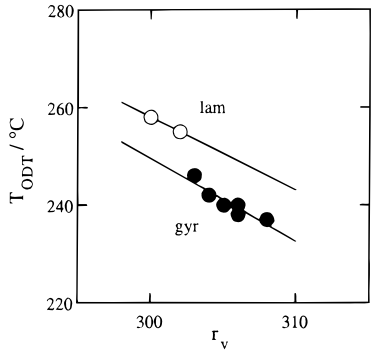

Figure 9. Order−disorder transition temperature versus copolymer chain length for blends of copolymers $E_{155}B_{76}$ and $E_{115}B_{103}$: data from Table 3.

persisted to the crystal−liquid boundary. We note that the ordinate values will be subject to systematic error arising in the determination of $\chi(T)$: see section 3.4. However, this uncertainty does not debar qualitative interpretation of the features of the diagram.

The lines on the diagram have been drawn with considerable freedom in order to highlight the observed features. Moving across the phase diagram from low to high ϕ_E and up the diagram from disorder to order (low to high χr_v, i.e., high to low T), these are (i) disorder to bcc at $\phi_E \approx 0.21$, at present defined by one point; (ii) disorder to hex; (iii) disorder to gyr, bounded at high χr_v (low temperature) by order−order transitions to either a true hex phase or to a morphology which could not be defined with certainty (possibly hpl and possibly coexisting hex and lam phases); (iv) disorder to lam; (v) disorder to gyr at $\phi_E \approx 0.71$, at present defined by one composition and bounded at high χr_v by an order−order transition to the lam phase; (vi) disorder to hex. Data points in a second bcc region (high ϕ_E) were not obtained in the present experiments. It is clear that a more detailed investigation of the concentration range $\phi_E = 0.68-0.78$ (gyr phase) should be rewarding, and this work is in hand. With regard to the hpl/biphasic region, an hpl phase is likely to be a highly metastable state,[27] while coexisting phases are a likely consequence of our use of blends to map out the phase diagram in that region (see section 3.3).

The phase diagram is asymmetric about $\phi_E = 0.5$. This is as expected. If χ is independent of ϕ_E, the symmetry of the phase diagram is controlled by parameter ϵ, i.e.

$$\epsilon = v_E b_B^2 / v_B b_E^2 \tag{7}$$

where v_E, v_B, b_E, and b_B represent the volumes and statistical lengths of the E and B units.[28] The diagram can be globally symmetrical only if $\epsilon = 1$. For the E/B system $\epsilon = 0.65$,[2,5] and the effect is to bias the phase diagram to the high-ϕ_E side. Further, a concentration dependence of χ may also contribute to asymmetry of the phase diagram. It has been shown that χ for the closely related poly(oxyethylene)−poly(oxypropylene) system is concentration dependent and that this biases the phase-separation boundary in that system toward high ϕ_E.[29]

As can be seen in Figure 8, the ODT boundary is not smooth. In particular, the transition between the disordered and gyroid phase occurs at higher χr_v than would be required for a smooth boundary between the lamellar and hexagonal regions. This reflects the observation that the ODT temperature of a gyroid phase is lower than that of a hexagonal or lamellar phase formed from a copolymer with the same segment length: see Table 3 and Figure 9. This same behavior was also observed for a polystyrene−poly(2-vinylpyridine) diblock copolymer system.[30]

The boundary predicted by self-consistent mean-field theory (see section 4.3 for details) is shown in Figure 8 as a dashed curve. Theory predicts (as it must) that $(\chi r_v)_c \approx 10.5$[7,8,21] at $\phi_E = 0.5$ compared with $(\chi r_v)_c \approx 14$ at $\phi_E = 0.5$ for the experimental boundary in Figure 8. Self-consistent mean-field theory has not yet been generalized to account for composition fluctuations. Since allowance was made for a fluctuating melt when treating the experimental data to determine χ, the difference between the experiment and theory is at least partly forced.

4.2. Comparison with Other Systems. The phase behavior of a number of block copolymer systems has been explored. The state of the field was reviewed in 1994 by Bates et al.,[31] who provided a number of illustrative phase diagrams, including those for diblock polyolefins and for polystyrene-*block*-polyisoprene (S_mI_n). A full account of the phase diagram for the S_mI_n system was published later.[19] More recently, phase diagrams have been reported for poly(ethylene-*alt*-propylene)-*block*-poly(dimethylsiloxane) $[(EP)_m(DMS)_n]$[15] and poly(oxyethylene)-*block*-poly(ethylethylene) $[E_m(EE)_n]$.[32] In respect of the review,[31] it should be stressed that the hpl phases, together with the related hexagonally modulated lamellar (hml) phase, are no longer considered to be equilibrium states. The hml phase may be nothing more than a fluctuating lamellar phase, as suggested in Yeung et al.[33] While hpl is clearly a distinct phase, careful experiments have found it to be a metastable state that eventually converts to the gyroid phase.[27] This negates the earlier report[31] that fluctuations are responsible for stabilizing the gyroid phase. It is now known that the stability of the gyroid phase derives from intermediate interfacial curvature compared to that of the lamellar and cylindrical morphologies coupled with a uniform interfacial curvature and domains of uniform thickness.[34]

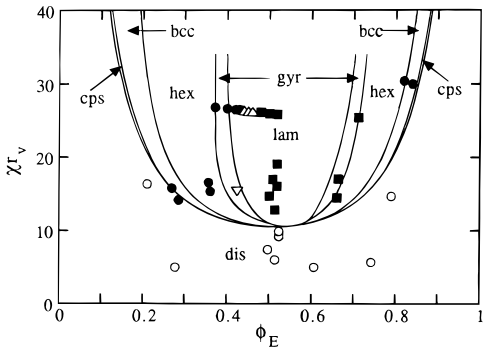

Figure 10. Positions of the E_nB_m diblock copolymers, calculated for a melt temperature of 70 °C with $\chi = 0.086\,44$, on a phase diagram calculated using the numerical procedure described by Matsen and Schick:[7] (○) copolymers with $T_m > T_{ODT}$ having only the disordered phase accessible; (●) hex phase; (△) hpl/biphasic region; (■) lam phase; (▽) gyroid phase. Data points for copolymers with ODT < 70 °C are necessarily missing from the diagram, most notably that for the bcc phase of copolymer $E_{40}B_{79}$: see Table 2 and Figure 8 for details.

There are obvious similarities between the present phase diagram (Figure 8) and those reported previously. This correspondence is most obvious in the comparison of the present phase diagram in Figure 8 with the phase diagram for copolymers S_mI_n set out in Figure 13 of ref 19 and also with that found by Vigild for $(EP)_m(DMS)_n$.[15] All three phase diagrams include stability regions for the gyroid regions. As noted above, the gyroid phase is now known to be stable in regions initially thought to be hpl.[27] Accordingly, it is possible that the gyroid phase is the equilibrium state in the region in Figure 8 where our samples were biphasic or hpl.

There are differences in molecular characteristics between S_mI_n and the E_mB_n and $(EP)_m(DMS)_n$ systems. Molar masses in the S_mI_n system are higher (with correspondingly higher block lengths): i.e., $M_n = 10\,000$−$80\,000$ g mol^{-1} compared with 4000−15 000 g mol^{-1} for the other two. This lower molar mass is accompanied (as it must be if microphase separation is to occur at similar values of χr_v) by higher values of χ. Reduced to the same segment volume of 100 cm^3 mol^{-1} and for $T =$ 100 °C, χ is 0.12 for S_mI_n but 0.21 for $(EP)_m(DMS)_n$ and 0.26 for E_mB_n. The corresponding value for $E_m(EE)_n$ copolymers[32] is 0.79.

Bates et al. have used parameter $\bar{N}$ of eq 5 calculated for identical reference conditions as an indicator of the importance of composition fluctuations in systems of different chemical composition.[31] Adopting their reference conditions ($\phi_E = 0.5$, $T = 150$ °C), we find a value of $\bar{N} \approx 800$ for E_mB_n, compared with 1100 for S_mI_n and 500 for $(EP)_m(DMS)_n$, i.e., rather similar values, consistent with the similarity of the phase diagrams of the three systems.

4.3. Comparison with Theory. A phase diagram has been calculated for an asymmetric copolymer ($\epsilon =$ 0.6) using the full self-consistent mean-field theory:[7] see Figure 10. In that method it is assumed that the blocks can be represented by incompressible Gaussian chains, but other restrictive approximations are avoided, e.g., the narrow interface and unit-cell approximations used by Helfand and Wasserman,[35,36] or the small basis set and truncated Landau expansion used in the random-phase approximation by Leibler.[21] Effects of polydispersity, finite persistence length, and concentration dependence of χ as well as the effect of thermally induced composition fluctuations in the copolymer melt are ignored. The three classical structures (body-centered cubic, hexagonal, and lamellar) are predicted, together with gyroid and close-packed sphere structures (cps, see Figure 10). For present purposes, this phase diagram is an improvement over that of Vavasour and Whitmore,[28] also calculated for $\epsilon = 0.6$ since that is based on the unit-cell approximation, and so is restricted to the classical structures.

The positions of the E_mB_n diblock copolymers on the phase diagram were calculated for $T = 70$ °C using a value of $\chi = 0.0864$ given by eq 4. The use of mean-field theory for both diagram and data points allows for some compensation of errors. Even so, as can be seen in Figure 10, the observed structures do not agree exactly with the theoretical predictions. In particular, the experiments display a larger asymmetry in the phase diagram than that predicted by theory. Nevertheless, the comparison is regarded as encouraging, particularly in the observations concerning the gyroid phase and the associated order−order transitions.

There are a number of features of mean-field theory and experiment which need to be improved before close agreement can be expected. Some of these are referred to above and are discussed in ref 8. We note that the small difference between the experimental value of $\epsilon =$ 0.65 and the value of $\epsilon = 0.60$ used in the calculations does not account for different degrees of asymmetry in the phase diagram.[37] Most important are fluctuation effects, which are ignored in the theory and only roughly assessed in our experiments, and the likely concentration dependence of χ, which is also ignored in the theory and seldom assessed by experiment.

Allowance for composition fluctuations can be made in the Landau theory for weakly segregated block copolymers. A broad region of the gyroid phase between lamellar and hexagonal phases is predicted for systems with small $\bar{N}$, with a direct transition between the disordered and gyroid phases, a feature not accounted for by self-consistent mean-field theory.[38]

5. Concluding Remarks

The use of E_mB_n copolymers carries certain advantages for investigation of microphase-separation behavior in block copolymer systems and comparison of experimental results with current theory.

(i) Compared with the carbanion chemistry used in the preparation of many block copolymers, the oxyanion chemistry used in the preparation of E_mB_n copolymers is relatively straightforward and robust. This is seen in the number of copolymers synthesized for the present work, which results in less reliance on blending than in the case of many other studies.

(ii) The chain lengths necessary for inducing phase separation are small, which is a consequence of the high value of the Flory−Huggins parameter in the E_mB_n system, e.g., roughly twice that reported for the S_mI_n system when compared at the same segment volume. This promotes rapid equilibration, with the result that the gyroid phase is prominent in the phase diagram; i.e., metastable hpl and biphasic regions are relatively unimportant.

Acknowledgment. Thanks are due to Dr. G.-E. Yu for invaluable help with the syntheses of the copolymers and to Dr. F. Heatley and Mr. K. Nixon for help with their characterization by NMR and GPC. Financial

support came from the Engineering and Physical Science Research Council (U.K.).

References and Notes

(1) For example, see: Kelarakis, A.; Havredaki, V.; Yu, G.-E.; Derici, L.; Booth, C. *Macromolecules* **1998**, *31*, 944 and references therein.
(2) Yang, Y.-W.; Tanodekaew, S.; Mai, S.-M.; Booth, C.; Ryan, A. J.; Bras, W.; Viras, K. *Macromolecules* **1995**, *28*, 6029.
(3) Ryan, A. J.; Fairclough, J. P. A.; Hamley, I. W.; Mai, S.-M.; Booth, C. *Macromolecules* **1997**, *30*, 1723.
(4) Mai, S.-M.; Fairclough, J. P. A.; Viras, K.; Gorry, P. A.; Hamley, I. W.; Ryan, A. J.; Booth, C. *Macromolecules* **1997**, *30*, 8392.
(5) Mai, S.-M.; Fairclough, J. P. A.; Hamley, I. W.; Matsen, M. W.; Denny, R. C.; Liao, B.-X.; Booth, C.; Ryan, A. J. *Macromolecules* **1996**, *29*, 6212.
(6) Bates, F. S.; Fredrickson, G. H. *Annu. Rev. Phys. Chem.* **1990**, *42*, 525.
(7) Matsen, M. W.; Schick, M. *Phys. Rev. Lett.* **1994**, *72*, 2660.
(8) Matsen, M. W.; Bates, F. S. *Macromolecules* **1996**, *29*, 1091.
(9) Bras, W.; Derbyshire, G. E.; Ryan, A. J.; Mant, G. R.; Felton, A.; Lewis, R. A.; Hall, C. J.; Greaves, G. N. *Nucl. Instrum. Methods Phys. Res.* **1993**, *A326*, 587.
(10) Ryan, A. J. *J. Therm. Anal.* **1993**, *40*, 887.
(11) Bras, W.; Derbyshire, G. E.; Clarke, S.; Devine, A.; Komanschek, B. U.; Cooke, J.; Ryan, A. J. *J. Appl. Crystallogr.* **1994**, *35*, 4537.
(12) Ryan, A. J.; Bras, W.; Mant, G. R.; Derbyshire, G. E. *Polymer* **1994**, *35*, 4537.
(13) Mai, S.-M.; Booth, C.; Nace, V. M. *Eur. Polym. J.* **1997**, *33*, 991.
(14) Zhao, J.; Majumdar, B.; Schulz, M. F.; Bates, F. S.; Almdal, K.; Mortensen, K.; Hadjuk, D. A.; Gruner, S. M. *Macromolecules* **1996**, *29*, 1204.
(15) Vigild, M. E.; Almdal, K.; Mortensen, K.; Hamley, I. W.; Fairclough, J. P. A.; Ryan, A. J. *Macromolecules* **1998**, *31*, 5702.
(16) Matsen, M. W.; Bates, F. S. *Macromolecules* **1995**, *28*, 7298.
(17) Hamley, I. W.; Koppi, K. A.; Rosedale, J. H.; Bates, F. S.; Almdal, K.; Mortensen, K. *Macromolecules* **1993**, *26*, 5959.
(18) Förster, S.; Khandpur, A. K.; Zhao, J.; Bates, F. S.; Hamley, I. W.; Ryan, A. J.; Bras, W. *Macromolecules* **1994**, *27*, 6922.
(19) Khandpur, A. K.; Förster, S.; Bates, F. S.; Hamley, I. W.; Ryan, A. J.; Bras, W.; Almdal, K.; Mortensen, K. *Macromolecules* **1995**, *28*, 8796.
(20) Hamley, I. W.; Fairclough, J. P. A.; Mai, S.-M.; Booth, C.; Ryan, A. J. submitted for publication.
(21) Leibler, L. *Macromolecules* **1980**, *13*, 1602.
(22) Fredrickson, G. H.; Helfand, E. *J. Chem. Phys.* **1987**, *87*, 697.
(23) Beech, D. R.; Booth, C. *J. Polym. Sci., Polym. Phys. Ed.* **1969**, *7*, 575.
(24) Booth, C.; Orme, R. *Polymer* **1970**, *11*, 626.
(25) Kugler, J.; Fischer, E. W.; Peuscher, M.; Eisenbach, C. D. *Makromol. Chem.* **1983**, *184*, 2325.
(26) Abe, A. In *Comprehensive Polymer Science*; Booth, C., Price, C., Eds.; Pergamon Press: Oxford, U.K., 1989; Vol. 2, p 55.
(27) Hadjuk, D. A.; Takenouchi, H.; Hillmyer, M. A.; Bates, F. S.; Vigild, M. E.; Almdal, K. *Macromolecules* **1997**, *30*, 3788.
(28) Vavasour, J. D.; Whitmore, M. D. *Macromolecules* **1993**, *26*, 7070; *Macromolecules* **1996**, *29*, 5244.
(29) Cooper, D. R.; Booth, C. *Polymer* **1977**, *18*, 171.
(30) Schulz, M. F.; Khandpur, A. K.; Bates, F. S.; Almdal, K.; Mortensen, K.; Hadjuk, D. A.; Guner, S. M. *Macromolecules* **1996**, *29*, 2857.
(31) Bates, F. S.; Schulz, M. F.; Khandpur, A. K.; Förster, S.; Rosedale, J. H.; Almdal, K.; Mortensen, K. *Faraday Discuss.* **1994**, *98*, 7.
(32) Hadjuk, D. A.; Kossuth, M. B.; Hillmyer, M. A.; Bates, F. S. *J. Phys. Chem. B* **1998**, *102*, 4269.
(33) Yeung, C.; Shi, A.-C.; Noolandi, J.; Desai, R. C. *Macromol. Theory Simul.* **1996**, *5*, 291.
(34) Matsen, M. W.; Bates, F. S. *Macromolecules* **1996**, *29*, 7641; *J. Chem. Phys.* **1997**, *106*, 2436.
(35) Helfand, E.; Wasserman, Z. R. *Macromolecules* **1976**, *9*, 879, **1978**, *11*, 960; **1980**, *13*, 994.
(36) Helfand, E. *J. Chem. Phys.* **1975**, *62*, 999.
(37) Matsen, M. W.; Bates, F. S. *J. Polym. Sci., Part B* **1996**, *35*, 945.
(38) Hamley, I. W.; Podneks, V. E. *Macromolecules* **1997**, *30*, 3701.

MA981089K